The Journal of Experimental Biology 207, 913-922
Published by The Company of Biologists 2004
doi:10.1242/jeb.00843

Kinematics and hydrodynamics of swimming in the mayfly larva

John Brackenbury

Department of Anatomy, University of Cambridge, Downing Street, Cambridge CB2 3DY, UK

e-mail: jhb1000@cam.ac.uk

Accepted 17 December 2003

Summary

The kinematics and hydrodynamics of free-swimming mayfly larvae (*Chloeon dipterum*) were investigated with the aid of a simple wake visualisation technique (tracer dyes) and drag measurements on dead insects. The basic swimming movement consists of a high-amplitude dorso-ventral undulation and, during continuous swimming, this produces a wake of ring vortices shed alternately to the dorsal and ventral sides of the body. The ring vortices propagate laterally away from the body at an angle of approximately 80° relative to dead aft of the swimming line. Thus, mayfly larvae, like damsel-fly larvae, resemble eels in producing a wake consisting of separate vortices that propagate laterally rather than the reverse von Karman vortex street characteristic of most caudal fin swimming fish. The thrust estimated from the momentum in the wake of swimming mayfly larvae was comparable with the drag measured on dead specimens. Possible sources of error in these estimates are discussed, but the conclusion is reached that even though only 14% of the total force generated by vortex production is directed forwards, it is still sufficient to account for the thrust required for steady locomotion.

Key words: larva, swimming, kinematics, vortex wake, drag, starting manoeuvre, mayfly, *Chloeon dipterum*.

Introduction

As Lighthill (1969) observed, most aquatic organisms with an elongated body form employ undulatory motion to propel themselves through the water. Depending on body size and swimming speed, as characterised by the Reynolds number, undulatory motion can generate thrust forces *via* viscosity or *via* acceleration of the water in contact with the propulsor surface. Propulsive force generation in larger fishes and cetaceans that swim in the range of Reynolds numbers of 10^4–10^8 is dominated by inertial forces of the medium and the body (Wu, 1977) whereas larval fishes (Hale, 1996) and the majority of invertebrate undulatory swimmers operate at Reynolds numbers of a few thousand at most. Invertebrates using an undulatory swimming style include nematodes (Gray and Lissman, 1964), leeches (Kristan et al., 1982), ascidian tadpoles (Chia et al., 1984; McHenry, 2001), lancelet larvae (Stokes, 1997; Jordan, 1992), ceratopogonid fly larvae (Nachtigall, 1961) and chironomid pupae (Brackenbury, 2000). Although Lighthill (1971) argued that most invertebrates swimming at intermediate Reynolds numbers (1–1000) would rely on viscous forces for their propulsion, Jordan's model of chaetognath swimming (Jordan, 1992) implies considerable force production through inertia even at Reynolds numbers of a few hundred. Models such as Jordan's can only be tested if information is available on the structure of the flow field in the vicinity of the moving animal, for it is only from such observations that an idea can be gained of the amount of momentum injected into the water.

Modern wake studies began with the vortex theories of Rayner (1979) and Ellington (1984), which attempted to describe how energy is organised in the wake. The essence of these theories is that bursts of vorticity released from the propulsor surface should be composed of closed vortex loops, often in the form of small-cored vortex rings, and the first structures of this kind were demonstrated (using stereophotography of neutrally buoyant bubbles) in bird flight (Spedding et al., 1984). Wake visualisation studies have confirmed that fish also transfer momentum into the water in a regulated manner although the precise structure of the wake depends on speed, swimming style and use of the caudal, dorsal and pectoral fins (McCutchen, 1977; Blickan et al., 1992; Muller et al., 1997, 2001; Wolfgang et al., 1999; Wilga and Lauder, 1999; Lauder, 2000; Liao and Lauder, 2000; Drucker and Lauder, 1999, 2000). As Videler (1993) postulated, the wake generated by a caudal fin swimmer consists of a chain of linked vortices in the form of a reverse von Karman street, but slow pectoral fin swimming and turning in sunfish (*Lepomis macrochirus*) produces discrete, unlinked ring vortices (Drucker and Lauder, 1999, 2000).

A recent study using a simple dye technique for wake visualisation showed that an invertebrate, undulatory swimmer – the damsel-fly larva – sheds discrete ring vortices to the side of the swimming path, one ring vortex per half-stoke (Brackenbury, 2002). This type of wake lacks a caudally directed thrust jet and is similar to that described in the eel (*Anguilla anguilla*; Muller et al., 2001), which, like the damsel-fly larva, uses a high-amplitude undulation generating high

lateral body velocities. In both cases, the ring vortices propagate away from the body at a very large angle (~70°) relative to the rear. Two other insect swimmers, the culicid larva and pupa (Brackenbury, 1999, 2001), also generate discrete ring vortices with each half-stroke but they propagate backwards much closer to the swimming line. Neither of these insects uses the undulatory method of swimming, but instead the body is subjected to simple side-to-side bending. The present study describes an invertebrate undulatory swimmer, the mayfly larva, that pushes water almost directly to the side rather than behind the body and, in this respect, resembles the damsel-fly larva. But, unlike the latter, which is a relatively slow swimmer, the mayfly larva swims as fast as specialised dytiscid water beetles of the same size. Therefore, among the questions to be asked in this study is how an apparently ineffective method of swimming can generate such high forward speeds.

Materials and methods

Final-stage larvae of *Chloeon dipterum* L. with a body length of approximately 1 cm (Table 1) were collected from freshwater ponds in the fenland district of north-west Cambridgeshire, UK. The insects were maintained indoors at temperatures of 17–22°C, in tanks containing water and detritus from the ponds of origin. Within one or two days of collection, individual larvae were transferred to a transparent container measuring 16 cm×8 cm×8 cm (width × depth × height) containing pond water to a depth of 6–7 cm. Swimming movements were recorded in daylight conditions with a Panasonic video camera (S-VHS format, horizontal resolution >400 lines at 25 frames s^{-1}) delivering 50 fields s^{-1} at shutter speeds of 0.00025–0.001 s. Additional data were obtained using a nac 200 high-speed video camera (nac Inc., Japan) with slave stroboscopic illumination delivering 200 fields s^{-1} (VHS format, horizontal resolution >210 lines). Despite its nominally similar resolution, the high-speed camera produced much poorer images than the Panasonic and, although the detailed inspection of movements was carried out using the Panasonic, the high-speed camera was used to confirm quantitative measurements of stroke rate. Videotapes were viewed on a cassette recorder with a single-field advance facility for detailed inspection of kinematic and hydrodynamic events. Swimming trajectories and dye movements were traced by hand directly from the video screen but no allowance was made for minor distortion of the images due to curvature at the edges of the screen. Flow visualisation followed the method previously described (Brackenbury, 2001, 2002), which made use of tracer dyes consisting of a harmless colouring agent (E122) suspended in water and glycerol (specific gravity of suspension 1.012 g ml^{-1}) or fresh cow's milk. The characteristic swimming behaviour of the larvae was taken into account in the design of the experiments. Mayfly larvae share several features with previously described damsel-fly larvae; both are negatively buoyant and prefer to rest near the bottom of the water, partially camouflaged by detritus.

Table 1. *Kinematic and hydrodynamic parameters of mayfly larvae during continuous swimming*

Body length (cm)	0.98±0.08 (12)
Swimming speed (cm s^{-1})	20.8±2.7 (20)
Swimming speed (BL s^{-1})	21.2±2.8 (20)
Stroke frequency (s^{-1})	26.9±3.0 (18)
Tail beat amplitude (BL)	0.26±0.05 (15)
Vortex momentum angle (deg.)	8.14±9.2 (18)[a]
	82.0±11.0 (15)[b]
	79.2±12.8 (48)[c]
Vortex external diameter (cm)	0.48±0.06 (20)[d]
	0.33±0.06 (20)[e]
Vortex ring diameter (cm)	0.30±0.05 (15)
Vortex jet velocity (cm s^{-1})	8.5±1.5 (27)

BL, body length. Values are means ± S.D. (*N*).

[a]Measured from bottom layer impressions; [b]measured during open water horizontal swimming; [c]measured during upward swimming; [d]measured at right angles to the vortex axis; [e]measured along the vortex axis.

Locomotory activity is generally of two kinds: horizontal swimming across the bottom, with the longitudinal axis of the body held a few millimetres above the bottom, and open-water swimming, upwards, downwards or in the horizontal direction. In the first series of visualisation experiments, a thin layer (approximately 1 mm) of milk was carefully laid on the bottom of the container through a syringe, and larvae swimming across the bottom left behind a trail of 'footprints' as evidence of their wakes. These trails were filmed from directly above the container, care being taken to exclude trails caused by physical contact between the undersurface of the body and the tracer. In practice, the latter could be readily identified: when a larva swam clear of the bottom, there was a clear delay between its passage over any particular point on the bottom and the eventual appearance of a footprint at that point. This delay represented the time for the wake disturbance to travel from the fish to the bottom. In cases of direct contact, movements of the larva produced immediate disturbances of the milk layer. In a second series of experiments, a more accurate method was used to visualise the wakes of larvae swimming in open water by dispensing tracer into the water in the form of a narrow (0.5–1.0 mm) streamer released from the barrel of a plungerless syringe mounted vertically above the container, with the tip of its needle just penetrating the surface and discharging slowly under gravity. The speed of descent of the streamers was 4–5 mm s^{-1}, equivalent to approximately 5% of the speed of the jets visualised in the wakes. In these experiments, the insects were recorded from the side of the container. In a third series of experiments, observations were made on insects performing starting manoeuvres from a position of rest on the bottom of the container. In some cases, the bottom was covered with a layer of milk in an attempt to visualise flows associated with these manoeuvres. Recording was performed, in separate experiments, from either above or from the side of the container. Altogether, approximately

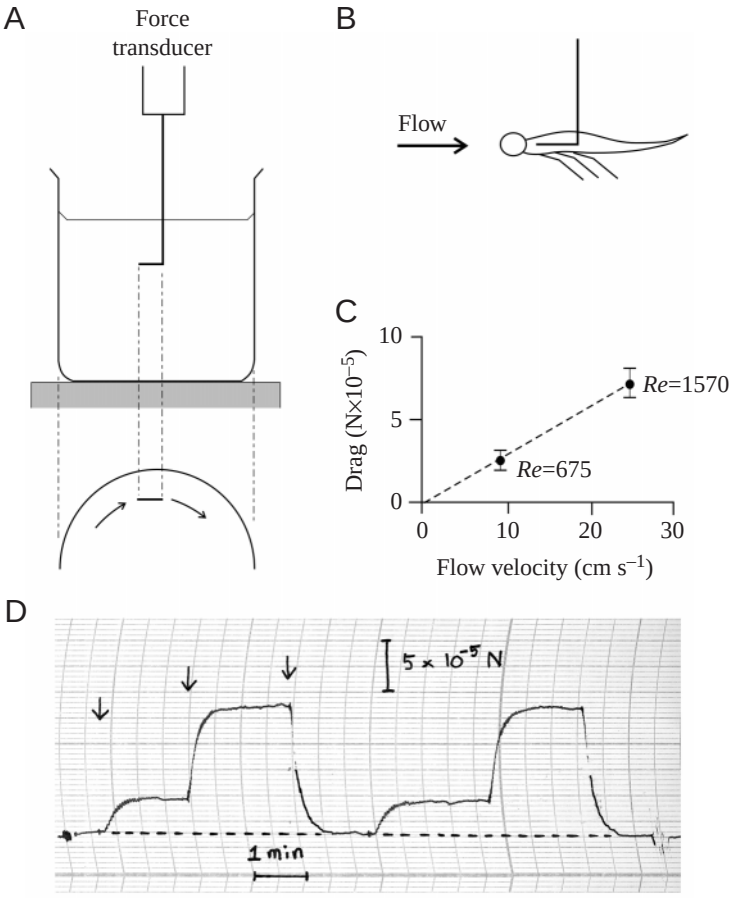

Fig. 1. Experimental technique for drag measurement in dead specimens. (A) Side view and (below) plan view of water-bath mounted on turntable and containing insect holder attached to force transducer. For ease of presentation, the insect holder has been enlarged: the length of the horizontal 'hook' was 3.5 mm, and the diameter of the vessel was 12 cm. Arrows in plan view indicate water flow. (B) Enlarged view of insect holder. (C) Experimental findings; see text for further details. (D) Original recordings of drag measurement. The first arrow on the left indicates the point at which the turntable was activated at the slower speed. Within approximately 1 min, a stable flow regime was established. At the point shown by the second arrow, the turntable was switched to the higher speed. The third arrow marks the point at which the turntable was switched off and flow steadily declined to zero. After a delay of 1 min, the series was repeated to give a duplicate set of recordings for this individual.

120–150 individuals were used in these three sets of experiments. Most of these were used in order to obtain a qualitative understanding of the relationship between kinematics and wake generation. Quantitative data were obtained from a sub-sample of ~50 individuals showing the greatest clarity of visual detail.

A final series of experiments was designed to measure the hydrodynamic drag on the bodies of dead insects. The insect was impaled on a stiff, 10 μm-diameter wire, the end of which was bent into a right-angled 'hook' (Fig. 1A). The other end of the wire was connected to a Grass FT03 force displacement transducer, the signal from which was displayed on a Grass 7D pen recorder. A steady flow regime was achieved by mounting a 12 cm-diameter vessel, containing water to a depth of 5 cm, on a two-speed turntable. Within approximately 1 min of starting the turntable, the water in the container attained solid body rotation. The impaled insect was immersed 2 cm below the surface of the water, at a distance of 4.5 cm from the centre of the container and orientated in line with the flow. At this point, the flow velocities were estimated to be 9.5 cm s^{-1} and 25.0 cm s^{-1} at the lower and higher turntable speed settings, respectively, and their values were confirmed by dropping dye immediately in front of the insect's head and filming its motion around the streamline. No account was taken in subsequent calculations for the slight curvature of the streamlines in the vicinity of the insect's body. In each experiment, duplicate measurements were made at both flow velocities, allowing ~2 min for equilibration of the readings.

The force measurement system was calibrated by rotating the transducer plus holder through 90° and suspending small weights from the end of the wire holder. The flow resistance of the immersed length of wire lying just above the mounted insect was measured by repeating the flow experiments using a simple length of wire (i.e. minus hook and insect), immersed to a depth of 2 cm. This value was then deducted from the original recordings. In total, successful duplicate measurements were obtained for 11 specimens, several others being discarded when the orientation of the insect altered during the course of the experiments.

Results

Continuous swimming

Kinematics and flow-field measurements

The tail fin of a *Chloeon* larva consists of three long, hair-fringed bristles that, unlike the tail fin of a fish, are held in the horizontal not the vertical plane. The bristles are down-curved but, since the larva rests with its abdomen slightly dorsiflexed (see 0 ms and 80 ms positions in Fig. 8), the tips of the bristles do not make contact with the substrate. During swimming, the body undulates in the median plane, so technically the tail beats up and down relative to the body rather than from side to side. Nevertheless, when the larva swims on its side, its slender, fusiform profile gives it a remarkably fish-like appearance, especially when viewed from above. As soon as swimming commences, the legs are trailed behind the body, presumably to reduce drag, and the lateral bristles of the tail fin become partially adducted, reducing the effective width of the tail fin to approximately 50% of its resting value. The tail beat frequency is very rapid (27 Hz), and the undulatory wave increases in amplitude from 0.09±0.03 body lengths (BL; N=13) at the head to 0.26±0.05 BL (N=13) at the fin tip. Further kinematic data are given in Table 1.

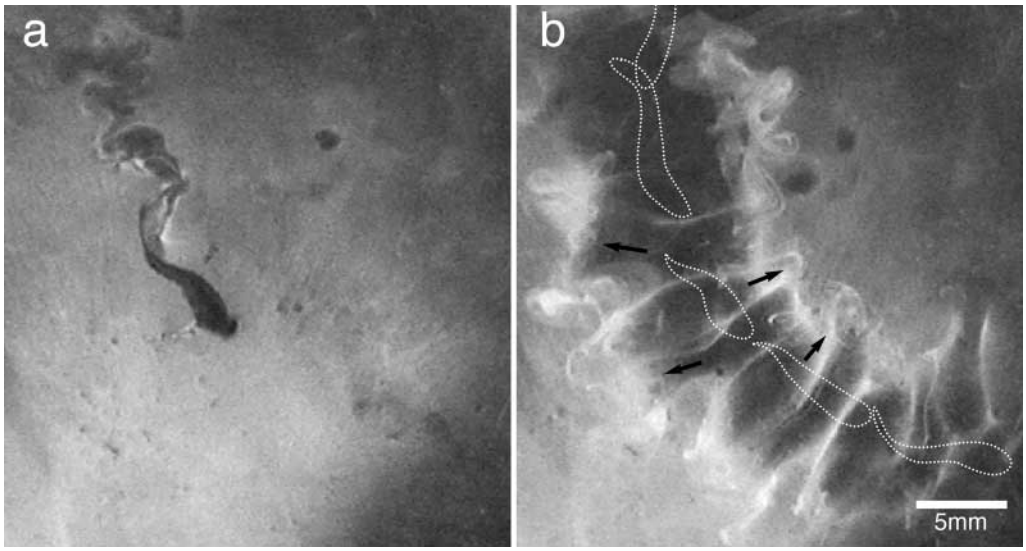

Fig. 2. Trail produced by the wake of a continuously swimming mayfly larva. The larva is swimming on its side just above the bottom layer of milk and is viewed from above. It is pursuing a slightly curved path from top left to bottom right. (a) The initial trace consists of a sinuous line coinciding with the motion of the tail fin. (b) The appearance of a fully formed trail 0.5 s after the events shown in a. Profiles of the larva are shown at successive 40 ms intervals. The mature trail consists of a ladder-like series of areas, each corresponding to a half-stroke, in which the general motion (as indicted by the arrows) of the dye is nearly at right angles to the swimming line.

Mayfly larvae swim either on their sides or in the upright position, and the wake created by the movements of the body leaves a different impression on the bottom layer of dye depending on which mode is used. Fig. 2 shows an example of the impression left by the wake of a larva swimming side-on to the bottom. Visual inspection from the side of the container showed that, as was often the case, the larva was moving parallel to the bottom with its body held clear of the bottom by a few millimetres. Initially, the area cleared of dye consists of a sinuous wave coinciding with the fin tip path (Fig. 2a). The main motion of the water thereafter is outwards away from the mid-line of the swimming path, and, for an individual half-stroke, this continues for 250–300 ms. The 'mature' wake impression consists of a ladder-like series of segments cleared of dye and separated from their neighbours by thin, more or less transverse lines of dye (Fig. 2b). Each segment corresponds to the wake generated during a single half-stroke, and the mean direction of the apparent flow within each segment was approximately 81° relative to the rear of the swimming line (Table 1). The pattern of impressions created by the wake of a larva swimming close to the bottom in upright mode was quite different. In this case, the dye was affected solely by the ventral half of the wake and consisted of a line of roughly circular areas, each of which started as a pinpoint and expanded within 40–60 ms to a circle with a mean diameter (measured transversely to the swimming line) of 0.49±0.08 BL (N=29; Fig. 3). The frequency of these circular impressions was 28.3±2.8 s^{-1} (N=11), which is not significantly different from the stroke frequency. The implication is that the chain of circular events was produced by alternate half-strokes performed to the ventral side of the body.

Unpredictable ground effects, and the fact that the bottom-layer technique can only produce a two-dimensional impression of a three-dimensional wake, meant that the findings of these experiments were not in themselves conclusive but could only be used to help interpret the results of the second series of open-water experiments. Fig. 4 shows an encounter between the wake of a larva swimming in open water and a dye streamer. In Fig. 4a, the larva is moving downwards in a 'seven o'clock' direction and the tail fin is within 20 ms of the completion of its dorsad swing. Approximately 40 ms on from Fig. 4a, a wake element intercepted the dye streamer and propagated outward from the swimming line. This element was a discrete ring vortex, and Fig. 4b shows dye being drawn into the trailing edge of the ring vortex, then travelling along the vortex axis and beginning to outline the leading edge. A further 0.22 s later (Fig. 4c), the dye has re-circulated into the main body of the vortex, revealing the vortex core. A second example of a dye-infiltrated vortex is shown in Fig. 5: the ellipsoidal shape of the vortex, the ring core and fluid flow into the trailing edge of the vortex are all evident. The swimming paths of the larvae in these experiments only rarely coincided with a streamer for long enough to allow consecutive ring vortices to be visualised, but one example is shown in Fig. 6. In total, approximately 40 individual ring vortices were identified that had penetrated a dye streamer 'head-on', allowing measurements of external radius parallel to the ring plane (r_p), external radius in the direction of the vortex axis (r_a), ring radius (r) and axial jet velocity ($\dot{V}_{jet}$; Fig. 7A). Although the vortex cores could be seen with relative ease and the opposite core centres could be approximately located by eye it was not possible to obtain a reliable estimate of core diameter. As was the case with ring vortices produced in the wakes of swimming culicids (Brackenbury, 2001), V_{jet} was measured from the consecutive positions of the dye front as it moved along the vortex axis after becoming drawn into the trailing edge at the start of the

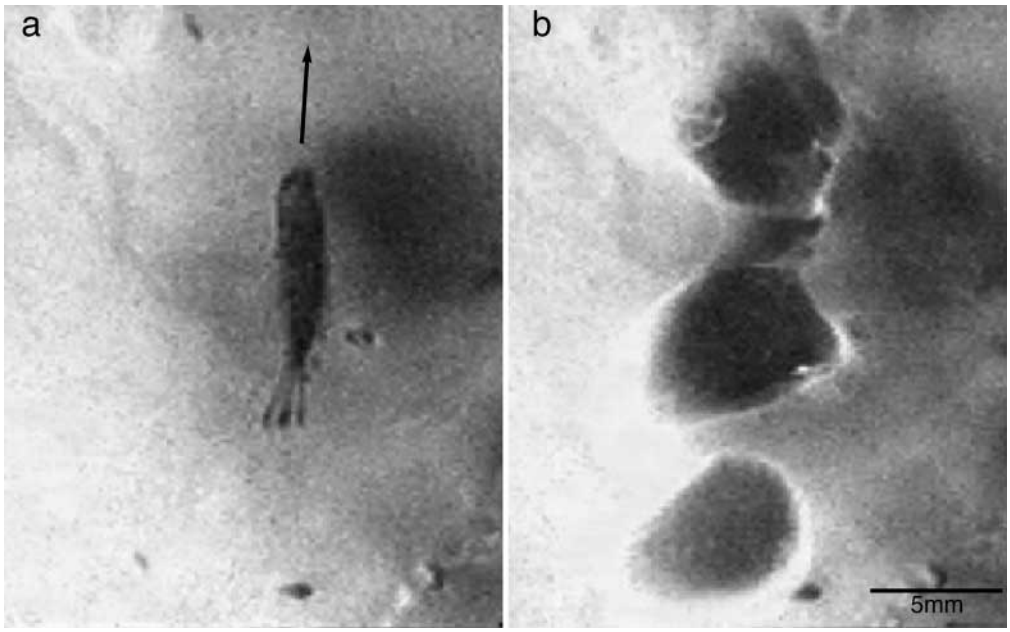

Fig. 3. Trail produced by the wake of a continuously swimming mayfly larva. The larva is swimming upright just above the bottom layer of milk and is viewed from above. (a) The larva is swimming in the direction indicated by the arrow: the larva is seen in dorsal view and the three tail fin bristles can be identified. At this point, there is no indication of the wake. (b) 0.4 s later, the larva has progressed beyond the field of view, and three roughly circular impressions have appeared in the bottom layer. As explained in the text, these were produced by three consecutive half-strokes executed to the ventral side of the swimming line.

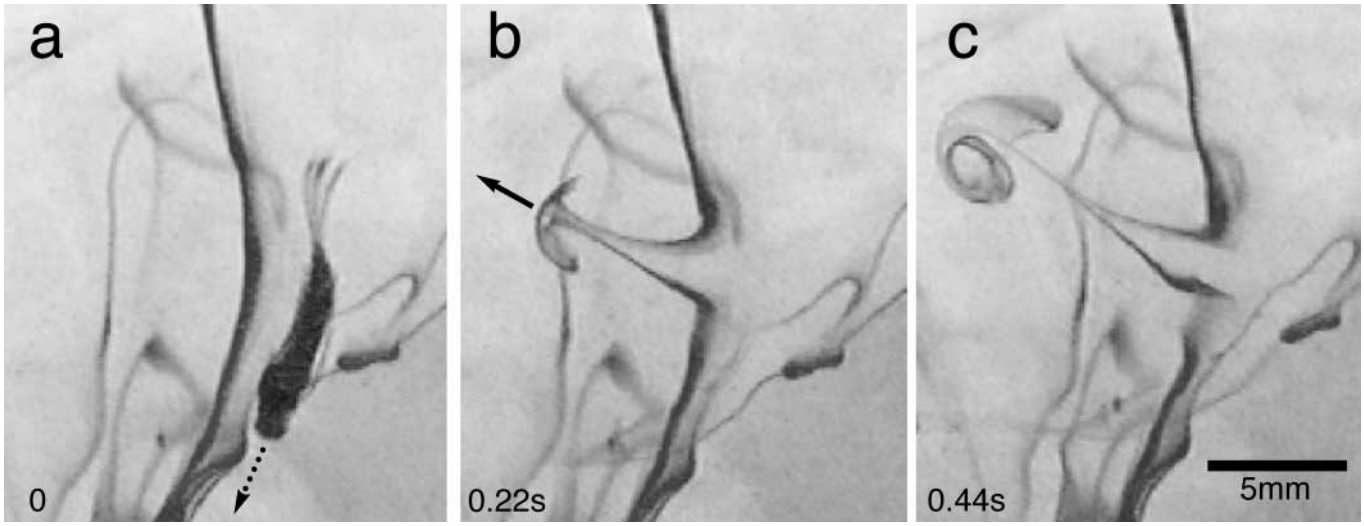

Fig. 4. Progressive visualisation of a discrete ring vortex shed from the tail fin of a swimming mayfly larva. In a, the larva is swimming in the direction of the arrow and is viewed from the side (dorsal to the left). The tail fin is within 20 ms of the completion of its dorsal half-stroke. To the left of the larva is a curved streamer. Subsequent frames (b,c) show the progressive outlining of the ring vortex shed from the tail as it penetrates the streamer. See text for more details. The arrow in b shows the direction of propagation of the ring vortex.

visualisation process. The movement of the dye front was most clearly discernible once it had reached the level of the ring plane, and this maximal value for axial $\dot{V}_{jet}$ is given in Table 1. This is the distance travelled by the dye front, in open-water fixed co-ordinates, in the particular 20 ms interval coinciding with its passage through the ring plane. Note that the ring vortex travels away from the swimming line at its own self-induced velocity and therefore the value given in Table 1 represents a summation of the propagation velocity and the axial flow velocity due to internal circulation within the vortex. In three instances, it was possible to establish a crude velocity profile of the dye front as it progressed along the vortex axis. The data points in Fig. 7B are given in vortex-fixed co-ordinates and therefore plot the re-circulatory component of the vortex jet. Velocity increases from zero at the trailing edge, reaches a maximum at the ring plane and decreases as dye re-circulates along the leading edge. This pattern is similar to that observed in culicid ring vortices and is approximately what would be expected in a 'classic' ring vortex. The mean value of V_{jet} at the ring plane for the three examples shown in Fig. 7B is approximately 4 cm s^{-1}, i.e. half the $\dot{V}_{jet}$ value shown in Table 1, which includes the propagation velocity. Although the data for comparison are limited, they suggest that approximately half the jet velocity is due to the propagation of

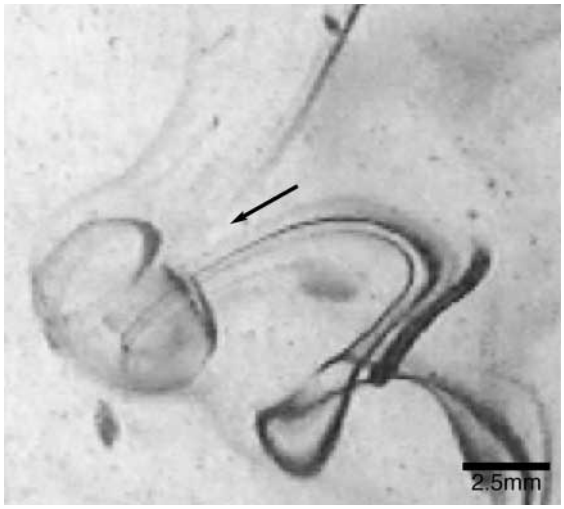

Fig. 5. A ring vortex approximately 0.5 s after penetrating a dye streamer. The arrow shows the direction of propagation of the ring vortex. Note the ellipsoidal shape of the vortex, the outlining of the vortex core and the continuing movement of dye into the trailing edge of the vortex.

the ring vortex and half is due to internal circulation, a result again roughly in agreement with findings on culicid ring vortices.

The momentum axis of the ring vortices, measured in the stroke plane (ϕ; Fig. 7A, right), did not differ significantly during horizontal or upward swimming (Table 1). These values were also not significantly different from the 'apparent' momentum axis values measured in the bottom-layer experiments.

Hydrodynamic drag

Original recordings from a single individual are shown in Fig. 1D, and data from all 11 experimental subjects are summarised in Fig. 1C. By extrapolation from Fig. 1C, the estimated drag at the normal swimming speed of 20.8 cm s^{-1} was approximately 6.5×10^{-5} N. Reynold's numbers entered into Fig. 1C are based on the body length minus the tail bristles [0.71± 0.04 cm (*N*=6)].

Transient manoeuvres

Mayfly larvae resting on the bottom display two kinds of escape manoeuvre in response to a threatening stimulus. In terms of the end result, the manoeuvres could be described as 'rapid start' and 'rapid turn about', although the two are very closely related. The threatening stimulus used in this study was a mild mechanical shock applied to the right side of the head or thorax. A rapid start begins with a dorsiflexion, which pulls the legs up from the substrate and arches the body so that the tail fin is brought into contact or near-contact with the dorsal surface of the head and thorax (20 ms position, Fig. 8A). Simultaneously, the larva rolls onto its left side and the anterior part of the body yaws to the left: these movements are particularly clear when the larva is seen in dorsal view

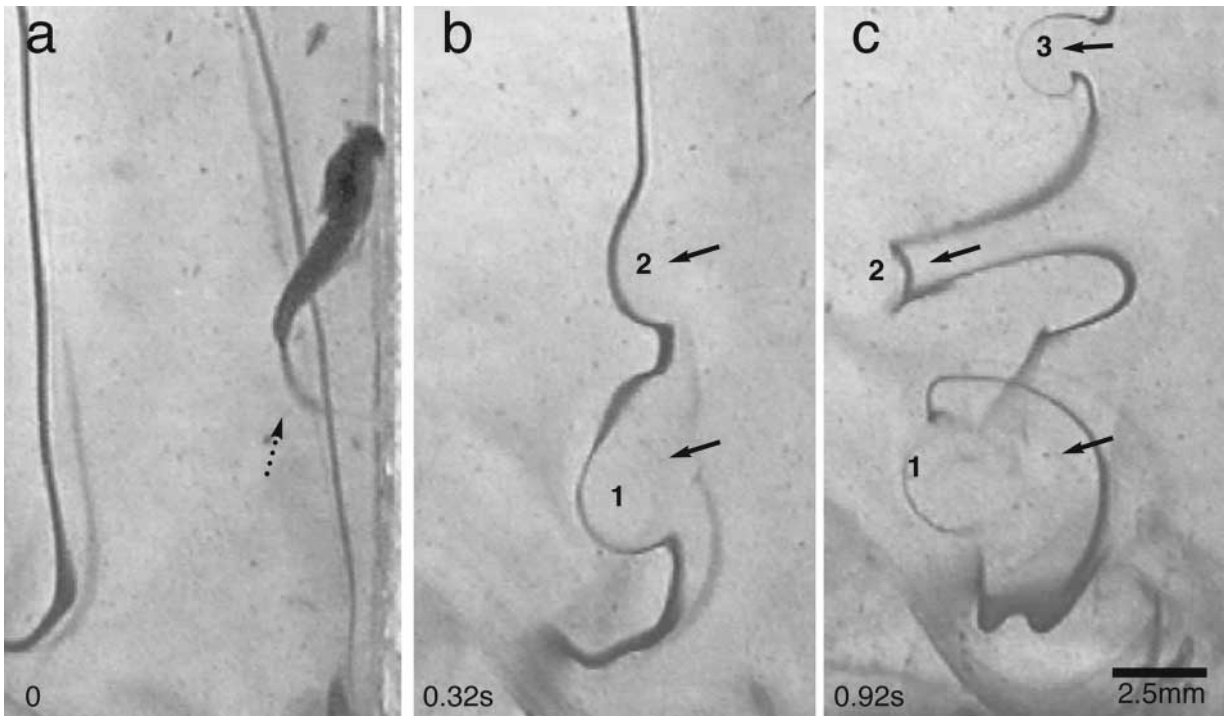

Fig. 6. Visualisation of a train of consecutive ring vortices shed to the dorsal side of the swimming line. The larva is swimming obliquely upwards, as indicated by the broken arrow in a, and is viewed from its right side (dorsal side is to the left of the profile). On the far left in a is a vertical dye streamer. b and c show stages in the penetration of the streamer by ring vortices released from the larva during consecutive dorsal half-strokes. The arrows in b and c indicate the direction of propagation of the ring vortices.

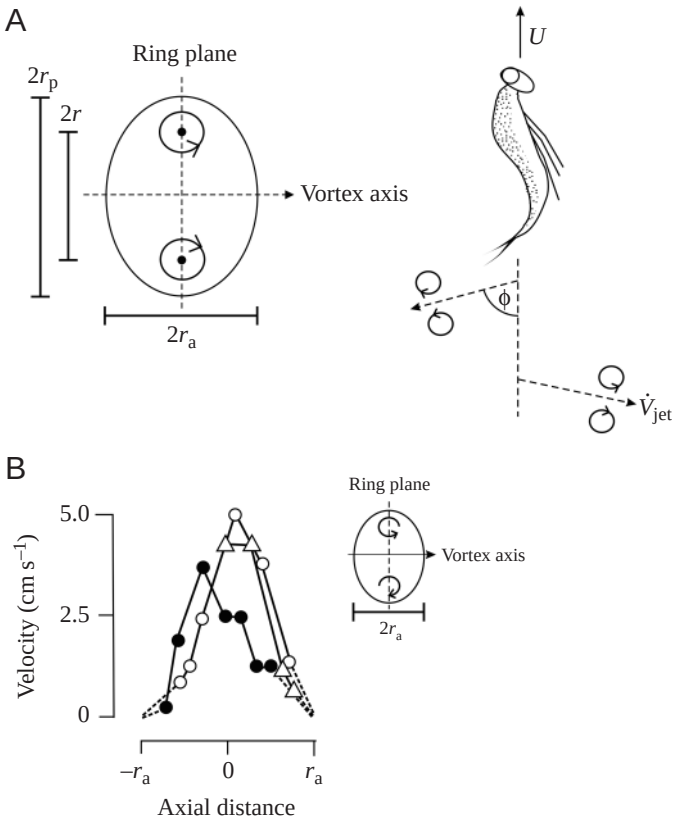

Fig. 7. (A) Flow variables measured during mayfly larval swimming. A scheme of an individual ring vortex is shown on the left and of the pattern of ring vortex shedding on the right. Abbreviations: r, ring radius; r_p, ring vortex radius measured at the ring plane; r_a, ring vortex radius measured along the vortex axis; $\dot{V}_{jet}$, jet velocity relative to the surrounding water measured at the ring plane; U, forward velocity; ϕ, momentum axis of the ring vortex in the median plane of the body. (B) Velocity profiles measured along the vortex axis in three separate ring vortices. The data represent the distance travelled by the dye front, during consecutive 20 ms intervals, as it progressed from the trailing edge to the leading edge of the ring vortex. The data are given in vortex fixed coordinates and therefore represent the re-circulatory component of the axial jet.

(Fig. 8D). As a result, by 40 ms from the start of the manoeuvre, the larva becomes pointed in a new direction. This part of the manoeuvre, characterised by dorsiflexion, can be termed stage 1. Extension (stage 2) now drives the body in the new direction (40 ms and 60 ms stages in Fig. 8A,D). The turning angle (yaw angle) varied from 40° to 160°, with a mean value of 112.4±33.8° (N=39; Fig. 8D). At the end of stage 2, a ring vortex was released from the body and this propagated in a direction approximately opposite to the line of exit of the larva from the manoeuvre. Subsequent swimming movements carried the larva away on its side with the long axis of its body held parallel to the bottom with its centre held 0.34±0.09 BL (N=8), or approximately 3 mm, above the bottom (Fig. 8A, 60 ms stage). Although the manoeuvre involves some movement of the body in the vertical plane during stage 1, the rapid start is essentially a turn and escape to the side. The durations of stages 1 and 2 were 25.5±7.6 ms (N=20) and 32.5±8.5 ms (N=20), respectively.

Stage 1 of the turn-about manoeuvre is identical to stage 1 of the rapid start. But, by the end of stage 2 (extension), the body has rolled back to its upright position and the legs, which have been trailing to this point, are re-extended to make renewed contact with the bottom (60 ms and 80 ms positions in Fig. 8B). As it lands on the bottom, the larva performs a partial dorsiflexion, restoring the abdomen to its normal resting configuration: this upward flick of the tail fin sheds a single ring vortex that propagates 19.2±9° (N=6) forward of the vertical (Fig. 8C, right). Since the reaction of the larval body to this vortex is downwards and backwards, it can be seen as a 'braking' vortex, counteracting the force of the initial propulsive vortex released at the end of stage 2.

Discussion

Continuous swimming

The interpretation of the findings of the open-water dye streamer experiments is consistent with a wake model in which separate ring vortices are shed above and below the body with alternate half-strokes and propagate almost at right angles to the swimming line (Fig. 7A). This model can also be reconciled with the findings of the bottom-layer experiments, which cannot in themselves be regarded as definitive but are at least supportive. In particular, the agreement between the external dimensions of the circular impressions shown in Fig. 3 (0.49 cm) and the external diameter of the ring vortices measured parallel to the ring plane (0.48 cm; Table 1) is consistent with laterally propagating ring vortices impacting on the bottom layer of dye.

The wake structure of the final-instar mayfly larva is similar to that previously described in the damsel-fly larva (Brackenbury, 2002). In both larvae, swimming movements produce a series of discrete ring vortices, one vortex per half-stroke, which are shed to alternate sides of the mean swimming line and propagate away from the body at a high angle relative to the rear: approximately 80° in the case of the mayfly and 70° in the case of the damsel-fly. Culicid larvae and pupae also generate a double row of discrete ring vortices but these convect along a line much closer to dead aft: approximately 26° (Brackenbury, 2001). The ability of culicid pupae to steer their vortices much more favourably to the rear appears to be related to their swimming kinematics; swimming is based not on an undulatory wave but on up and down bending of the body, which induces large body rotations in the pitching plane (Brackenbury, 1999). Consequently, although the abdomen sweeps through a full circle about the head, the body rotations continuously re-align the tail fin so that it beats in a fore–aft direction (relative to the direction of swimming) rather than up and down. The ring vortex is shed when the tail fin has reached its most caudal position relative to the body, and the vortex propagates primarily backwards rather than to the side of the swimming path. By contrast, the ring vortex of the mayfly and

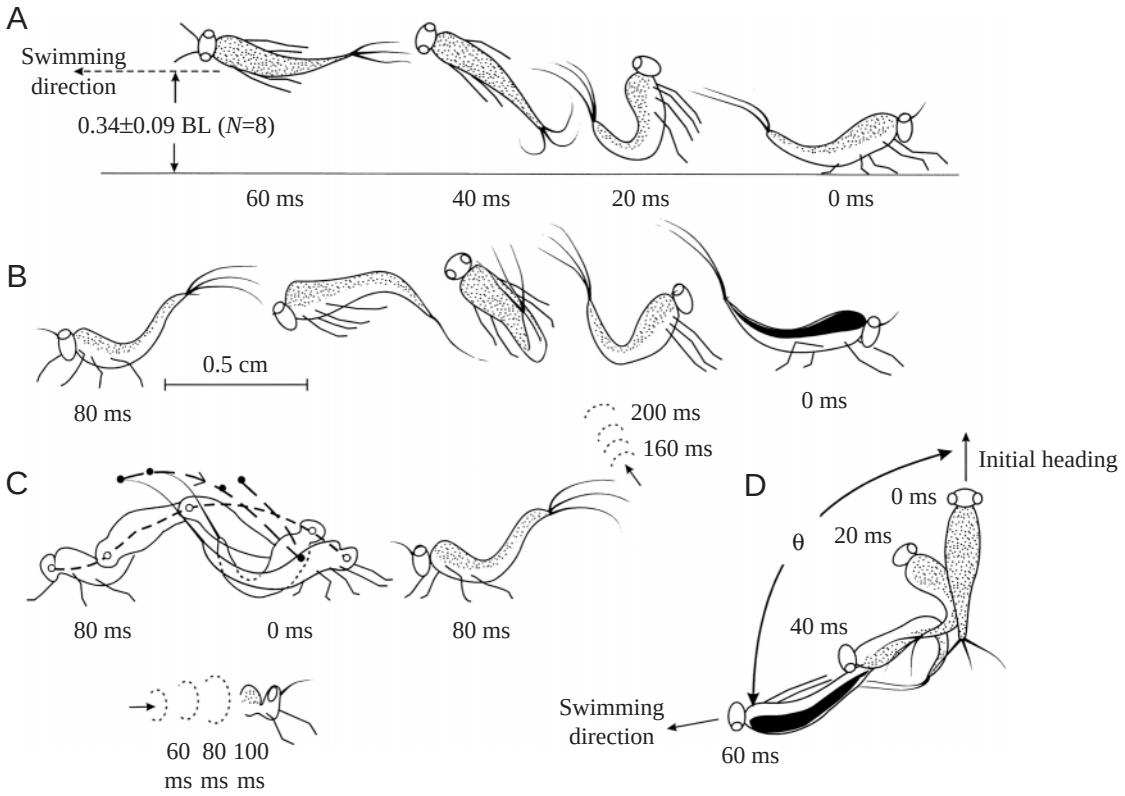

Fig. 8. Kinematics of rapid-start (A,D) and turn-about (B,C) manoeuvres. Resting positions of the larvae are indicated by 0 ms, and the insects are viewed from the side and facing to the right of the page. The dorsal surface of the body is stippled for ease of identification during the following manoeuvres. In each case, the larva receives a light touch to the right side of its head. Details are given in the text. C shows a turn-about manoeuvre in fixed co-ordinates (left). Filled and open circles represent the motion of the fin tip and head, respectively, at 20 ms intervals. The two drawings below and on the right, respectively, show the start and finish positions of the body during a turn-about. Dashed outlines plot the motion of ring vortices released during the extension phase of the manoeuvre and during the final upward tail-flick, respectively. Arrows show the direction of propagation of the ring vortices. (D) Dorsal view of a larva performing a rapid start; θ, turning angle.

damsel-fly larvae is released when the tail fin is at its most lateral position, and it propagates almost directly to the side. None of the above insects produces an aft-flowing jet such as that seen in the wake of continuously swimming fish that use the caudal fin for swimming and that consists of a reverse von Karman vortex street of linked vortices with a jet zigzagging between (Blickan et al., 1992; Muller et al., 1997; Wolfgang et al., 1999). Insect wakes are more like that described in the intermittently swimming Danio *Brachydanio rerio* (McCutchen, 1977) and the continuously swimming eel (Muller et al., 2001). The latter authors also cite other examples of swimming organisms generating laterally propagating ring vortices including *Brachydanio albolineatus*, a water snake (*Natrix natrix*) and a leech.

The digital particle image velocimetry images obtained by Muller et al. (2001) showed a double vortex shed to the side of the swimming line with each half-stroke that was interpreted as a ring vortex. The ring vortex was formed by contributions from a body wave and a tail wave, the latter being essentially a stop–start vortex associated with fin tip reversal at the stroke transition. The body wave generates semi-circular flow between the anterior crests and posterior troughs in the body contour, the vortex being massaged caudally along the body before joining the tail flow (Muller et al., 2001; Wolfgang et al., 1999). The large sideways component of momentum in the ring vortices of eels results in part from the high lateral velocities of the body surface associated with the transmission of the high-amplitude body wave. This condition also applies to mayfly and damsel-fly larvae, both of which have high tail beat amplitudes (mayfly, 0.26 BL; damsel-fly, 0.41 BL). According to Muller et al. (2001), the eel-like swimming pattern is a compromise between thrust and efficiency, where neither of these factors is particularly high. The propulsive efficiency of damsel-fly swimming, calculated independently from hydromechanical modelling and flow field measurements, was 0.65–0.67 compared with values of 0.7–0.8 in continuously swimming fish (Alexander, 1999). The propulsive efficiency of mayfly larvae is probably low since only 14–17% of the estimated force generated in reaction to the ring vortex is directed forwards.

Despite this, the larvae swim at speeds equivalent to those of specialised diving beetles of comparable body length (Nachtigall, 1977). During level swimming, a momentum balance must exist between the larva and its wake. The

downward component in the wake must balance the upward momentum in the body, exactly counteracting the force of gravity. Backward momentum in the wake must be balanced by forward momentum in the body overcoming the force of drag. Is there sufficient forward momentum in the visible wake of swimming mayfly larvae to account for forward movement?

Following the argument outlined in the previous study of damsel-fly swimming (Brackenbury, 2002), the momentum (M) of an axi-symmetric ring vortex can be given by:

$$M = \rho\pi r^2\Gamma\,, \tag{1}$$

where ρ is the density of water ($1000\,kg\,m^{-3}$), Γ is the circulation in the vortex, equal to the line integral of the tangential velocity component (V) around a curve enclosing the vortex core (Spedding et al., 1984; Drucker and Lauder, 1999). Since:

$$\Gamma \cong V_{jet} r_a\,, \tag{2}$$

and

$$M \cong \rho\pi r^2 V_{jet} r_a\,, \tag{3}$$

the mean force (F) on the propulsor surface associated with the production of the ring vortex is equal to the mean rate of change of momentum in the vortex:

$$F = M/t\,, \tag{4}$$

where t is the period of one half-stroke. Forward thrust is therefore:

$$F_t = F\cos\varnothing\,, \tag{5}$$

where $\varnothing$ is the momentum angle of the jet measured in the horizontal plane.

Taking values of r, r_a, V_{jet} and $\varnothing$ from Table 1 and a t value of 18 ms yields a forward thrust of 6.0×10^{-5} N. The measured drag on the bodies of dead mayfly larvae, extrapolated to the normal swimming speed, was 6.5×10^{-5} N, a value very close to the drag on the bodies of dytiscid beetles with similar body lengths and swimming speeds (Nachtigall, 1977): for example, *Agabus bipustulatus* (body length 9.5 mm; speed 20 cm s^{-1}; *Re* 1900; drag ~7×10^{-5} N) and *Agabus chalconatus* (body length 8.3 mm; speed 17 cm s^{-1}; *Re* 1400; drag ~5×10^{-5} N). Nachtigall found that drag was proportional to velocity^2, but only for larger dytiscids swimming at Reynolds numbers of 5000 and above. This is well above the range of Reynolds numbers relevant to mayfly larval swimming where, as Fig. 1C shows, Newton's Law of resistance (drag $\propto$ velocity^2) does not predominate.

The similarity between thrust and drag estimates in mayfly larvae appears to satisfy the need for a momentum balance during swimming, but these data cannot be taken at face value. It seems unlikely that the drag on the body of a dead larva is the same as that experienced by a living insect, with its continuously changing profile. The drag estimated will have been influenced by the slight curvature of the streamlines in the vicinity of the body: over the insect's body length, the mean direction of flow will have changed by approximately 10°. A further source of error may be inherent in the wake model, which is based on a 'classic' small-cored ring vortex; although the ring radius and the external radii of the vortex could be readily ascertained, it was not possible to measure the core radius. With these qualifications in mind, it can at least be concluded that the results of the present study are consistent with the findings in the previous studies of a momentum balance in swimming culicid and damsel-fly larvae.

Rapid-start manoeuvre

Two rapid-start manoeuvres have been identified in damsel-fly larvae: the 'flex' and the 'twist' (Brackenbury, 2002). The flex resembles the C-start of fish both kinematically and hydrodynamically and consists of a rapid flex/unflex movement in the horizontal plane. The twist is more complex, involving some movement in the vertical plane, which rolls the insect onto its side. In both cases, the insect exits from the manoeuvre at an angle of up to 160° from the original heading. A twisting damsel-fly larva dorsiflexes then flexes to one side, rolling the body onto its side (stage 1); it then extends (stage 2), accelerating the body in the new direction. It will be seen that this sequence of events is almost identical to that outlined in Fig. 8 for the mayfly larva. In both larvae, the tail fin makes brushing contact with the head at the end of stage 1, and extension results in the shedding of a single ring vortex approximately opposite to the line of body exit from the manoeuvre. The mayfly manoeuvre, however, is three times as fast: stages 1 and 2 together last 58 ms compared with 156 ms in the damsel-fly larva. The kinematics of damsel-fly rapid starts was found to be comparable, both in the timing and the geometrical changes in body shape, with the C-start of larval salmon (*Oncorhynchus tshawystscha*; Hale, 1996). The lowest body length limit investigated by Hale was 1.5 cm, and in this case the combined duration of stages 1 and 2 was 150–200 ms. This is comparable to the speed of response of a 2 cm-long damsel-fly larva but is much slower than the response of a 1 cm-long mayfly larva.

The mayfly larval 'turn about' cannot simply be interpreted as rapid start that fails to translate in continuous swimming. Before the end of stage 2, the larva has prepared for renewed contact with the ground by re-extending its legs and rolling its body back to the upright position. As a final adjustment, it then flicks the tail to produce a stopping vortex (Fig. 8C). All these features indicate that the 'turn about' is a calculated manoeuvre, intended solely to turn the larva away from the stimulus, but falls short of an attempt at escape. The behavioural parameters that govern the threshold between 'turn' and 'escape' are not known but presumably depend on the nature and intensity of the stimulus.

I wish to thank the Rutherford Appleton Laboratories, Oxford, for the loan of high-speed imaging equipment and Mrs Dee Hughes for art work.

References

Alexander, R. McN. (1999). *Energy for Animal Life.* Oxford: Oxford University Press.

Blickan, R., Krick, C., Zehren, D. and Nachtigall, W. (1992). Generation

of a vortex chain of a subundulatory swimmer. *Naturwissenschaften* **79**, 220-221.

Brackenbury, J. H. (1999). Regulation of swimming in the *Culex pipiens* (Diptera, Culicidae) pupa: kinematics and locomotory trajectories. *J. Exp. Biol.* **202**, 2521-2529.

Brackenbury, J. H. (2000). Locomotory modes in the larva and pupa of *Chironomus plumosus* (Diptera, Chironomidae). *J. Insect Physiol.* **46**, 1517-1527.

Brackenbury, J. H. (2001). The vortex wake of the free-swimming larva and pupa of *Culex pipiens* (Diptera). *J. Exp. Biol.* **204**, 1855-1867.

Brackenbury, J. H. (2002). Kinematics and hydrodynamics of an invertebrate undulatory swimmer: the damsel-fly larva. *J. Exp. Biol.* **205**, 627-639.

Chia, F. S., Buckland-Nicks, J. and Young, C. M. (1984). Locomotion of marine invertebrate larvae: a review. *Can. J. Zool.* **62**, 1205-1222.

Drucker, E. G. and Lauder, G. V. (1999). Locomotor forces on a swimming fish: three-dimensional vortex wake dynamics quantified using digital particle image velocimetry. *J. Exp. Biol.* **202**, 2393-2412.

Drucker, E. G. and Lauder, G. V. (2000). Wake dynamics and fluid forces of turning manoeuvres in sunfish. *J. Exp. Biol.* **204**, 431-442.

Ellington, C. P. (1984). The aerodynamics of hovering insect flight. V. A vortex theory. *Phil. Trans. R. Soc. Lond. B* **305**, 115-144.

Gray, J. and Lissman, H. W. (1964). The locomotion of nematodes. *J. Exp. Biol.* **41**, 135-154.

Hale, M. E. (1996). The development of fast-start performance in fishes: escape kinematics in the Chinook salmon (*Oncorhynchus tshawystscha*). *Am. Zool.* **36**, 695-709.

Jordan, C. E. (1992). A model of rapid-start swimming at intermediate Reynolds numbers: undulatory locomotion in the chaetognath *Sagitta elegans. J. Exp. Biol.* **163**, 119-137.

Kristan, W. B., McGirr, S. J. and Simpson, G. V. (1982). Behavioural and mechanosensory neurone responses to skin stimulation in leeches. *J. Exp. Biol.* **96**, 143-160.

Lauder, G. V. (2000). Function of the caudal fin during locomotion in fishes: kinematics, flow visualisation, and evolutionary patterns. *Am. Zool.* **40**, 101-122.

Liao, J. and Lauder, G. V. (2000). Function of the heteroceral tail in white sturgeon: flow visualisation during steady swimming and vertical manoeuvreing. *J. Exp. Biol.* **203**, 3585-3594.

Lighthill, M. J. (1969). Hydrodynamics of aquatic animal locomotion. *Annu. Rev. Fluid Mech.* **1**, 413-446.

Lighthill, M. J. (1971). Large-amplitude elongated-body theory of fish locomotion. *Proc. R. Soc. Lond. B* **179**, 125-138.

McCutchen, C. W. (1977), Froude propulsive efficiency of a small fish, measured by wake visualisation. In *Scale Effects in Animal Locomotion* (ed. T. J. Pedley), pp. 339-363. London, New York, San Francisco: Academic Press.

McHenry, M. J. (2001). Mechanisms of helical swimming: asymmetries in morphology, movement and mechanics of larvae of the ascidian *Distaplia occidentalis*. *J. Exp. Biol.* **204**, 2959-2973.

Muller, V. K., Van den Heuvel, B. L. F., Stamhuis, E. J. and Videler, J. J. (1997). Fish foot-prints: morphometrics and energetics of the wake behind a continuously swimming mullet (*Chelon labrosus* Risso). *J. Exp. Biol.* **200**, 2893-2900.

Muller, V. K., Smit, J., Stamhuis, E. J. and Videler, J. (2001). How the body contributes to the wake in undulatory fish swimming: flow fields of a swimming eel (*Anguilla anguilla*). *J. Exp. Biol.* **204**, 2751-2762.

Nachtigall, W. (1961). Zur locomotionsmechanik schwimmender Dipterenlarven. I. Mitteilung: Schwimmen ohne Ruderorgane: Ceratopogoniden und Chironomiden. *Z. Vergl. Physiol.* **44**, 509-522.

Nachtigall, W. (1977). Swimming mechanics and energetics of locomotion of variously sized water beetles – Dytiscidae, body length 2 to 35 mm. In *Scale Effects in Animal Locomotion* (ed. T. J. Pedley), pp. 269-283. London, New York, San Francisco: Academic Press.

Rayner, J. M. V. (1979). A vortex theory of animal flight. Part 1. The vortex wake of a hovering animal. *J. Fluid Mech.* **91**, 607-730.

Spedding, G. R., Rayner, J. M. V. and Pennycuick, C. J. (1984). Momentum and energy in the wake of a pigeon (*Columba livia*) in slow flight. *J. Exp. Biol.* **111**, 81-102.

Stokes, M. D. (1997). Larval locomotion of the lancelet *Branchiostoma floridae. J. Exp. Biol.* **200**, 1661-1680.

Videler, J. B. (1993). *Fish Swimming*. London: Chapman and Hall.

Wilga, C. D. and Lauder, G. V. (1999). Locomotion in sturgeon: function of the pectoral fins. *J. Exp. Biol.* **202**, 2413-2432.

Wolfgang, M. J., Anderson, J. M., Grosenbaugh, M. A., Yue, D. K. P. and Triantophyllou, M. S. (1999). Near-body flow dynamics in swimming fish. *J. Exp. Biol.* **202**, 2302-2327.

Wu, T. Y. (1977). Introduction to the scaling of aquatic animal locomotion. In *Scale Effects in Animal Locomotion* (ed. T. J. Pedley), pp. 203-232. London, New York, San Francisco: Academic Press.